JUL 8 '63

[redacted]

Copy
NASA TM X-720

NASA TM X-720

GROUP 4
Downgraded at 3 year intervals; declassified after 12 years

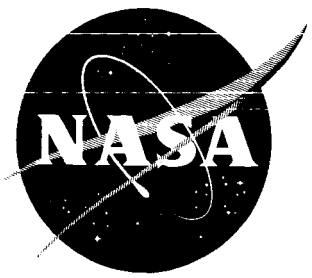

[redacted]

TECHNICAL MEMORANDUM

X-720

DESIGN AND COLD-AIR EVALUATION OF A FOUR-STAGE 8-INCH-MEAN-DIAMETER REVERSE-FLOW REENTRY TURBINE

By David G. Evans

Lewis Research Center
Cleveland, Ohio

LIBRARY COPY

JUL 8 1963

LEWIS LIBRARY, NASA
CLEVELAND, OHIO

CLASSIFICATION CHANGED
To Unclassified
By authority of H.G. Maines
Date 4-6-1972
per mr

CLASSIFIED DOCUMENT - TITLE UNCLASSIFIED

This material contains information affecting the national defense of the United States within the meaning of the espionage laws, Title 18, U.S.C., Secs. 793 and 794, the transmission or revelation of which in any manner to an unauthorized person is prohibited by law.

NATIONAL AERONAUTICS AND SPACE ADMINISTRATION
WASHINGTON

July 1963

[redacted]

NASA TM X-720

DECLASSIFIED

NATIONAL AERONAUTICS AND SPACE ADMINISTRATION

TECHNICAL MEMORANDUM X-720

DESIGN AND COLD-AIR EVALUATION OF A FOUR-STAGE 8-INCH-MEAN-DIAMETER REVERSE-FLOW REENTRY TURBINE*

By David G. Evans

SUMMARY

The design and performance characteristics of a reentry turbine incorporating a reverse-flow reentry system was investigated. The four-stage 8-inch-mean-diameter turbine was designed for a total- to static-pressure ratio of 20.5, a blade- to jet-speed ratio of 0.20, a first-stage arc of admission of 20.6°, and an equivalent mean blade speed of 385 feet per second.

At design speed and pressure ratio, the equivalent specific-work output was 44 Btu per pound at a static efficiency of 0.61. These values corresponded to design values of 46 and 0.64, respectively.

Interstage flow measurements made at design speed and pressure ratio indicated that near-design flow conditions were obtained between the second and third stages and between the third and fourth stages. Temperature and pressure ratios across the first stage were less than the design values and across the second stage were greater than the design values, so that one approximately compensated for the other. The temperature ratio across the fourth stage was slightly less than the design value. The static-pressure distribution throughout the turbine indicated that at design speed the second-, third-, and fourth-stage stators were choked at turbine total- to static-pressure ratios of 9.2, 13.9, and 20.5, respectively. The first-stage stator operated choked at all pressure ratios and speeds investigated.

INTRODUCTION

A research program has been in progress at the Lewis Research Center to investigate the design and performance characteristics of reentry turbines. The program is part of an overall investigation of both conventional and unconventional multistage high-specific-work low-weight-flow turbines designed for auxiliary-power and turbodrive applications.

In order to minimize total system weight in such applications, the turbine

*Title, Unclassified.

DECLASSIFIED

DECLASSIFIED

must be able to convert a maximum of its propellant energy to useful work. A high turbine-inlet-propellant enthalpy and a high turbine pressure ratio and efficiency are therefore required. Multistage turbines must be considered in order to utilize high pressure ratios efficiently, with the assumption that turbine speeds are limited either by blade-stress limitations or by other requirements of the system.

Reentry turbines were considered at length during the investigation because of the suitability of their unique design features to the requirements. Multistaging is accomplished by passing the flow through a single rotor several times, which reduces many of the mechanical problems associated with multiple rotors. Reentry ducts located in segments around the rotor annulus direct the flow between successive stages. The last stages cool the rotor, which allows for higher turbine-inlet temperatures and, hence, higher inlet enthalpies or higher blade speeds, generally, than would be possible for conventional turbines.

The cold performance of three so-called "crossover" reentry turbines investigated at Lewis is reported in references 1 to 3. These turbines had reentry systems that directed the flow over the rotor and thereby provided flow in the same direction through each stage. The crossover design permitted minimizing the unadmitted annulus areas between stages.

The length of the crossover reentry ducting, however, frequently contributed to losses in efficiency and considerably increased the overall weight, size, and complexity of the turbine. One means of overcoming these objections was utilization of the so-called "reverse-flow" reentry-type turbine, wherein the reentry system reenters the flow on the same side of the rotor from which it is discharged. Successive reentry ducts located on alternate sides of the rotor direct the flow through the rotor in opposite directions. Such designs usually result in equal rotor-blade inlet and outlet angles and symmetric rotor-blade and channel profiles. One such unit investigated was a small two-stage reverse-flow reentry turbine designed for auxiliary-drive applications. The performance of this turbine is reported in reference 4.

The subject four-stage turbine was designed to investigate further the performance characteristics of the reverse-flow reentry-type turbine. The design of the turbine was directed more toward turbopump-type applications than toward auxiliary-drive applications. The selection of four stages was arbitrary, but the use of an even number of stages simplified the test installation by allowing the turbine inlet and exhaust sections to be on the same side of the turbine. The turbine had a mean blade diameter of 8 inches and a stator blade height of 0.60 inch, which resulted in a blade radius ratio of 0.86. The criterion used in the design of the reentry system was that the system added a minimum to the size, weight, and complexity of the turbine. This criterion resulted in a reentry system that diffused the flow leaving each stage of the rotor to a relatively low velocity before directing it to the next stage.

The results of the design study and of the overall and interstage performance as obtained in cold air over an appropriate range of speeds and pressure ratios are presented.

DECLASSIFIED

DECLASSIFIED

TURBINE DESIGN

The design procedure used for the four-stage reentry turbine was formulated from an unpublished interstage flow analysis of the three-stage reentry turbine (ref. 1). The analysis was based on interstage flow measurements taken during that investigation. In the analysis, interstage flow-leakage losses significantly affected the stage and overall performance of the turbine. In the four-stage-turbine design procedure, therefore, the effects of interstage flow-leakage losses on stage weight flow, temperature, and pressure were computed and accounted for in the design. The procedure herein differs from that used in references 1 to 3, where stage flow conditions were computed with the assumption that all the turbine flow entered each stage with no leakage between stages. The present method, therefore, accounts more realistically for stage leakage effects in the determination of stage work, pressure ratios, velocity diagrams, and area ratios. The general design procedure is outlined in detail in appendixes A and B.

A schematic diagram of the turbine is shown in figure 1. Flow enters the turbine at station 0 and is staged four times through the single rotor to the turbine exit at station 15.

Overall Requirements

The turbine was designed for the following overall requirements. The values are corrected, where noted, to equivalent air conditions at the turbine inlet (station 0, fig. 1), that is, inlet-total temperature of 518.7° R and inlet pressure of 2116 pounds per square foot absolute.

Equivalent specific-work output, $\Delta h/\theta_{cr}$, Btu/lb	46
Equivalent mean blade speed, $U_m/\sqrt{\theta'_{cr}}$, ft/sec	385
Equivalent rotational speed, $N/\sqrt{\theta_{cr}}$, rpm	11,040
Speed-work parameter, λ	0.128
Equivalent weight flow, $w\sqrt{\theta_{cr}}\ \epsilon/\delta$, lb/sec	0.1195

(All symbols are defined in appendix C.)

Turbine weight flow was computed such that the resulting turbine with its 8-inch mean diameter and 0.60-inch blade height would have a total admitted flow area of 300° around the rotor annulus. The selection of 300° was arbitrary, but for four stages it resulted in a 15° separation between stages, which was considered about minimum for this design.

Turbine static efficiency, as noted in appendix B, was obtained by adjusting the static efficiency determined experimentally for the three-stage reentry turbine (ref. 1) by an amount estimated to account for the design differences between the three-stage and the four-stage turbines. The value of the overall static efficiency η used was 0.64, which resulted in an overall total- to static-pressure ratio p'_0/p_{15} of 20.5.

DECLASSIFIED

DECLASSIFIED
CONFIDENTIAL

Interstage Requirements and Assumptions

The losses in total pressure assumed across the various components of the turbine are given in table I. The procedure used to obtain these values, as well as the other interstage requirements and assumptions, is noted in appendix A.

The percentage of stator weight flow and flow-leakage loss present at each stage is given in table II.

The specific-work output per stage required to satisfy the stage velocity diagram requirements and overall work requirements (outlined in appendix A) are given in table III. Because less than 100 percent of the flow was available for staging, the total stage equivalent specific-work output, 56 Btu per pound, exceeded the overall equivalent specific-work requirement of 46 Btu per pound. The resulting speed-work parameter per stage λ_s is also given in the table.

The values of rotor total efficiency assumed for each stage are given in table IV. The level of efficiency was consistent with the previously established turbine overall total- to static-pressure ratio of 20.5. The variation in efficiency reflects an assumed effect of the variations in work, leakage, and reaction among the four stages. Stage efficiencies were not required, since stator and diffuser losses were accounted for in the total-pressure-loss assumptions (table I).

The resulting design free-stream velocity diagrams, which satisfy the preceding requirements and assumptions, indicate the degree of reaction across all blade rows (fig. 2). Rotor inlet and outlet blade angles are 40° from the tangential direction resulting in 100° of turning. All flow velocities are subsonic. A first-stage stator throat critical velocity ratio slightly below choke, $(V/V_{cr})_{1,t}$ of 0.95, resulted in a free-stream stator-outlet velocity ratio of $(V/V_{cr})_1$ of 0.93. Higher throat velocities up to choke would have resulted in less reaction across the first-stage segment of the rotor. There was approximately 11° of negative whirl at the outlet of the fourth stage, $(V_u/V_{cr})_{14}$ of 0.10.

The design static- and total-pressure variations through the turbine as ratios of the inlet total pressure p_0' are shown in figure 3. The total-pressure variation between each stage is indicative of the loss assumptions noted in table I and of the stage work and efficiency assumptions noted in tables III and IV. The static-pressure variation is indicative of the total-pressure variation and the critical velocity ratio V/V_{cr} at each station (fig. 2).

The design total-temperature variation through the turbine presented as a ratio of the inlet total temperature is shown in figure 4. The change in temperature across each diffuser section is indicative of a weighted average that was made of the leakage flows entering the diffuser at temperatures above or below the main stream with the main stream flow leaving the rotor.

DECLASSIFIED
CONFIDENTIAL

DECLASSIFIED
CONFIDENTIAL

Blade Design

The mean-diameter-stator nomenclature for all stages is given in figure 5. Because the same nontwisted blades were used for each stage, the blade-setting angle α and pitch s were varied with stage to obtain the correct flow angles and area ratios. These variations were slight, as noted in the figure, and the resulting blade channels were all smoothly convergent to a throat t, which was normal to both blade surfaces and was located at the trailing edge of the pressure surface. The suction surface was straight from the throat to the trailing edge. Throat areas, degrees of admission, and percent admission values computed in the previous section are also noted in figure 5.

The nomenclature for the rotor is given in figure 6. The design requirements for the blading were (1) a short axial chord to minimize flow-leakage losses due to pumping, (2) a wide enough channel to allow for easy machineability, but (3) an ample blade solidity to minimize suction-surface-flow deceleration. The blade sections also had to be nontwisted and symmetrical with equal inlet and outlet angles. The resulting design that best satisfied these criteria had a blade chord of 0.400 inch and a blade spacing of 3°, which resulted in a total of 120 blades and a mean blade solidity of 1.91.

In general, the blade-layout procedure corresponded to the method outlined in reference 5. A single mean-section blade design rather than a three-section design was used. Because the blade leading edge changed sides with each stage, both ends of the blades were designed as leading edges in the manner prescribed in the reference. Flow continuity across the rotor and flow equilibrium in the radial-axial plane and across the blade channel from the suction surface to the pressure surface were satisfied by use of the quasi-three-dimensional method of reference 6.

The resulting suction- and pressure-surface profiles were constant from hub to tip. Blade thickness was constant from the tip- to the mean-radius sections; however, a linear increase in blade thickness of 0.009 inch was made from the mean- to the hub-radius sections, as shown in figure 6(b). The tapered portion was required to provide sufficient blade rigidity to withstand the alternate aerodynamic loading and unloading of the blades with each stage and the various vibration-exciting frequencies caused by the partial unloadings from stator wakes. These frequencies varied with stator spacing and, hence, with stage.

A rotor tip clearance of 0.015 inch and an axial clearance of 0.020 inch on each side of the rotor was used (fig. 6(c)). The blade surface and midchannel velocity distribution for the last stage is shown in figure 7. The distribution was similar for all other stages and indicated almost no deceleration of the flow along the blade suction surface inside the channel.

Reentry Duct Design

Figure 1 shows schematically the configuration of the reentry system. The reentry ducts were designed to decelerate the flow leaving the rotor to a low velocity in a parabolic diffuser 1 inch long with an area ratio of $3\frac{1}{3}$ to 1. The

DECLASSIFIED
CONFIDENTIAL

DECLASSIFIED
CONFIDENTIAL

flow was then directed and reaccelerated by a $3\frac{1}{3}$-to-1 reduction in area to the next stage stators. The diffusers were located downstream of stations 2, 6, and 10 as are noted in the figure. The diffuser at the turbine exit, stations 14 to 15, had an area ratio of 2.5 to 1.

The circumferential offset of the flow in passing between the rotor inlet and outlet was computed to be 5.6°. The reentry ducts were therefore offset from the preceding stage stators by this amount.

APPARATUS, INSTRUMENTATION, AND PROCEDURE

The turbine components are shown in figure 8. The rotor was machined from a stainless-steel forging. The blade channels were electrically disintegrated to a tolerance within 0.001 inch of their design shape. The stator blades were ground from steel bar stock to the same tolerance and located in slots that were disintegrated through the stator rings and brazed in place. An exploded view of the turbine assembly showing the relative locations of the various parts and stations is shown in figure 9.

A photograph of the assembled turbine mounted in the facility is shown in figure 10. The means of mounting the turbine was unique to the facility. The turbine inlet was connected to a 4-inch vertical pipe and 90° elbow welded to the turbine exhaust pipe. The turbine was operated with dry pressurized air from the laboratory combustion-air system. Before entering the turbine, the air was passed through a filtering tank, a steam heat exchanger, an electric heater, a pneumatically operated inlet control valve, a calibrated ASME thin-plate orifice, and a screen. The air leaving the turbine was exhausted through a hydraulically operated throttling valve to the laboratory altitude exhaust system.

The power output of the turbine was transmitted through a 4-to-1 speed-reducing-gearbox cradle mounted to a direct-current dynamometer. Powers were measured with a pneumatic load cell calibrated before and after each performance test. Turbine speeds were measured with a magnetic pickup and a 60-tooth gear mounted on the rotor shaft in conjunction with an electronic tachometer.

Overall and interstage pressure measurements were made from static-pressure taps located on the turbine-inlet duct, exhaust duct, and reentry ducts (fig. 1). The measurements were recorded in inches of mercury on well-type manometers. Temperatures were measured with bare wire thermocouples located in the same areas and were recorded directly in degrees Fahrenheit on a self-balancing potentiometer. Flow velocities in the areas of instrumentation were generally below a critical velocity ratio of 0.1.

The turbine was operated at an inlet pressure of 65 pounds per square inch absolute and at a temperature of 280° F. The performance was obtained from data over a range of speeds and pressure ratios. Speeds were varied from 25 to 110 percent of the design value. Pressure ratios were varied from 6 to 48 by varying the outlet static pressure.

Turbine bearing and disk windage losses were obtained by replacing the rotor

CONFIDENTIAL
DECLASSIFIED

DECLASSIFIED

with a bladeless disk and motoring the turbine with the dynamometer to 100 percent design speed. Pressures measured in the turbine casing on either side of the turbine disk during performance testing were duplicated to simulate the disk windages losses and bearing thrust loadings. The resultant torque, measured with the pneumatic load cell, amounted to 9.3 percent (15 in.-lb) of the shaft torque output of the turbine at design speed and pressure ratio.

The turbine efficiency was computed as the ratio of the actual rotor-blade output (shaft output plus bearing and disk windage losses) to the ideal blade output. The ideal blade output was obtained from the National Bureau of Standards tables (ref. 7) for the measured values of turbine-inlet total temperature and pressure and turbine-outlet static pressure. Turbine specific-work output, speed, weight flow, and torque were corrected to standard NACA sea-level equivalent air conditions.

RESULTS AND DISCUSSION

Overall Performance

Overall turbine performance is presented in figures 11 to 14 and is based on the rotor-blade output (shaft output plus bearing and disk windage losses) mentioned previously. In figures 11 and 12, the equivalent specific-work output $\Delta h/\theta_{cr}$ and static efficiency η are shown for 100-percent design speed over the range of total- to static-pressure ratios P_r investigated from 6 to 48. At the design total- to static-pressure ratio of 20.5, the equivalent specific-work output was 44 Btu per pound (fig. 11) at a static efficiency of 0.61 (fig. 12). These values compared reasonably well with the design values of 46 and 0.64, respectively. The design equivalent specific work of 46 Btu per pound and the turbine limiting value of equivalent specific work of 47 Btu per pound were obtained at total- to static-pressure ratios of approximately 28 and 40, respectively.

In figure 13, the static efficiency is replotted against the blade- to jet-speed ratio ν at design speed and at the design total- to static-pressure ratio of 20.5. Experimental points are plotted from 25 to 110 percent design speed and from total- to static-pressure ratios of 6 to 48. The general shape of the curves approximates those of conventional axial-flow and crossover multistage reentry turbines. A peak static efficiency of 0.62 was obtained at a blade- to jet-speed ratio of 0.22, which was relatively close to the design point values of 0.61 and 0.20, respectively.

Turbine weight-flow measurements taken over the range of speeds and pressure ratios investigated indicated that a choked-flow condition was obtained across the first-stage stator. This compared with the design flow velocity ratio at the first-stage-stator throat $(V/V_{cr})_t$ of 0.95, which was slightly below choke. The choked equivalent weight flow was 0.118 pound per second, which was 1.3 percent below the design value of 0.1195 pound per second. This discrepancy was due in part to fabrication tolerances that resulted in a first-stage-stator throat area 1.0 percent smaller than the design value.

In figure 14, the equivalent shaft and blade torque $\tau\epsilon/\delta$ is shown plotted

DECLASSIFIED

DECLASSIFIED
CONFIDENTIAL

against percent design speed at the design total- to static-pressure ratio of 20.5. Experimental points were obtained from 25 to 110 percent of the design speed. Extrapolation of the blade-torque curve to zero speed indicated a breakaway torque of approximately 1.72 times the design-speed torque. The variation in blade torque with speed was approximately linear, as with conventional axial-flow and crossover reentry multistage turbines. The turbine bearing and disk windage losses account for the difference between the two curves.

The overall performance of the turbine is summarized in table V. The performance results are tabulated three ways: as measured in the cold-air tests, as corrected to NACA equivalent air conditions, and as corrected to an example hot-operating condition. The hot-operating condition, selected arbitrarily, corresponds approximately to hydrogen-oxygen propellants burning at an oxidant-to-fuel ratio of about 1.03. In the example, the resulting mean blade speed is somewhat higher than present conventional turbine design practice allows. Blade speeds approaching this value are possible if advantage is taken of the reduced operating temperatures unique with reentry-type turbines, and of the recent advances made in materials technology. However, only a five-point penalty in efficiency would result if mean blade speeds were reduced to 1450 feet per second, which would correspond to a blade- to jet-speed ratio of 0.152 (fig. 13).

Interstage Measurements

Interstage pressure and temperature measurements made during the performance evaluation of the turbine are presented in figures 15 and 16 and cover the same range of speeds and approximately the same values of pressure ratio noted previously for overall performance. In figure 15, the variation of station-static- to inlet-total-pressure ratio between stages is shown at design speed over the range of turbine pressure ratios investigated. The measurements indicated that near-design pressures were obtained between the second and third stages and between the third and fourth stages. Underexpansion across the first stage and overexpansion across the second stage, as compared with the design value, almost exactly compensated for each other. The measurements also indicated that the second-, third-, and fourth-stage stators were choked at turbine total- to static-pressure ratios of 9.2, 13.9, and 20.5, respectively. Essentially no variation in the static-pressure distribution was observed over the range of speeds investigated.

The pressures measured on both sides of the rotor disk at the design pressure ratio of 20.5 are also noted in figure 15 (stations a and b). The small difference between the pressures is indicative of a small axial-thrust loading; however, the general level of the pressures was slightly below that expected. If it is assumed that the design pressure ratio was obtained between stations 9 and 11 (fig. 3), the pressures at stations 9 and b would be equal, which would eliminate flow leakage across the labyrinth at station 9. In the design, a 1-percent labyrinth flow leakage was assumed from station b to station 9 (table II).

In figure 16, the variation of station- to inlet-total-temperature ratio among the four stages is shown at design speed over the range of turbine pressure ratios (fig. 16(a)) and at design pressure ratio (20.5) over the range of speeds

CONFIDENTIAL
DECLASSIFIED

DECLASSIFIED
CONFIDENTIAL

investigated (fig. 16(b)). Figure 16(a) indicates the same trends as noted in the pressure-distribution curves of figure 15. Near-design flow conditions were obtained in the second and third reentry ducts. Less-than-design work (temperature drop) was obtained across the first stage, which was nearly compensated for by greater-than-design work output across the second stage. The temperature ratio across the fourth stage was also less than the design value, which may have been caused by the higher than design temperature of the case leakage flow leaving the first stage and entering the last stage. Figure 16(b) indicates a fairly consistent reduction in stage work (temperature drop) with decreasing speed for each stage.

No conclusions were drawn concerning the underexpansion of the flow across the first stage. Possibly, the flow leakage or pressure losses assumed across the first stage were excessive and led to underexpansion of the flow. The flow across the first stage of the reverse-flow reentry turbine of reference 4 also underexpanded. It was noted that in the crossover reentry turbines of references 1 and 3 where 100 percent weight flow was assumed across the stages, the flow across the first stage overexpanded. The flow across the first stage of the turbine of reference 2 expanded as designed.

SUMMARY OF RESULTS

The results of the investigation of the four-stage 8-inch-mean-diameter reverse-flow reentry turbine designed for a pressure ratio of 20.5 and an equivalent rotational speed of 11,040 rpm are summarized as follows:

1. At design speed and pressure ratio, the equivalent specific-work output was 44 Btu per pound at a static efficiency of 0.61. These values corresponded to design values of 46 and 0.64, respectively. A limiting value of equivalent specific-work output of 47 Btu per pound was obtained above a total- to static-pressure ratio of approximately 40.

2. Torque-speed characteristics of the turbine are comparable with conventional axial-flow and crossover multistage reentry turbines. Zero speed breakaway torque was approximately 1.72 times design speed torque at design pressure ratio.

3. Near-design flow conditions were measured in the second and third reentry ducts. Considerable underexpansion of the flow and reduction in work, as compared with the design value, was observed across the first stage. These conditions were nearly compensated for by an overexpansion of the flow and a resultant increase in work across the second stage. The second-, third-, and fourth-stage stators were choked at turbine pressure ratios of 9.2, 13.9, and 20.5, respectively. The first-stage stator operated choked over the range of speeds and pressure ratios investigated.

Lewis Research Center
National Aeronautics and Space Administration
Cleveland, Ohio, November 30, 1962

DECLASSIFIED
CONFIDENTIAL

DECLASSIFIED

APPENDIX A

GENERAL DESIGN PROCEDURE FOR FOUR-STAGE REENTRY TURBINE

As noted in the TURBINE DESIGN section, the design procedure for the turbine was formulated from an unpublished interstage flow analysis made of the three-stage reentry turbine investigated in reference 1. This procedure involved a total of nine steps in determining stage temperatures, pressure ratios, velocity diagrams, weight flows, and area ratios. The steps were as follows:

(1) Turbine overall specific work and speed were assumed commensurate with the general turbine size and stage requirements noted in the INTRODUCTION, that is, four stages, a mean blade diameter of 8 inches, and a stator-blade height of 0.60 inch.

(2) Total-pressure losses were assumed across the first-stage stator, between the stations within the reentry system (fig. 1), and at the turbine exit. The values assumed are given in table I. The stator loss assumptions were made commensurate with the nominal level of flow velocities computed in step (9). An iterative process was required between steps (2) and (9). Likewise, the loss in total pressure assumed across each diffuser section reflected an assumed recovery of between 30 and 50 percent of the velocity head entering the diffuser. The diffuser at the turbine exit (stations 14 to 15), which was not part of the reentry system, had a higher assumed recovery of approximately 60 percent because of a lower area ratio.

(3) Turbine static efficiency was computed from the known performance of the three-stage reentry turbine (ref. 1) corrected for the differences in work and speed (loading), stage number (step (1)), total-pressure losses (step (2)), and improvements in flow leakage and interstage spilling losses. The considerations included in this adjustment and their effect on obtaining a final estimate of static efficiency are given in appendix B.

(4) From the value of specific work assumed in step (1) and the static efficiency assumed in step (3), the overall total- to static-pressure ratio was computed.

(5) The percentage of radial leakage through the rotor-rim axial-clearance space was obtained from the unpublished three-stage-turbine flow analysis modified to account for the differences in clearance between the two turbines and for the fact that the four-stage turbine had a labyrinth seal (fig. 6(c)), whereas the three-stage turbine did not. These values are given in table II. The percentage of weight flow pumped between stages within the rotor annulus was computed from the equation

$$w_p = \rho_{av} \times \text{blade height} \times \text{blade chord} \times U_m \times \varphi$$

where ρ_{av} was averaged across the blade chord for each stage. Values for the blade chord and for φ (the term accounting for blade blockage within the rotor annulus) were assumed at this point in the design and later were checked against

DECLASSIFIED

DECLASSIFIED

rotor-blade layouts. The circumferential leakage values in table II indicate that the percentage of flow pumped into each stage was assumed to be equal to the amount pumped out of the adjacent stage.

(6) The percentage of weight flow entering and leaving each stage other than through the turbine inlet or reentry system was computed from the percentage of weight-flow loss assumptions made in step (5) to obtain the total amount of flow available for expansion across each stage. The resulting values at each stage stator are given in table II.

(7) Values of equivalent specific-work output per stage were assumed such that the resulting turbine-exit temperature including the mass-averaged effects of stage leakage matched the overall specific-work requirement (step (1)). In addition, various work splits per stage were considered in order to obtain the following stage velocity-diagram characteristics:

(a) Moderate reaction (flow acceleration) across all blade rows to minimize flow losses (ref. 6)

(b) Sonic (choked) or near-sonic velocity at the first-stage stator throat

(c) Subsonic velocities throughout the rest of the turbine

(d) Zero tangential velocity at the turbine exit

The resulting values assumed for equivalent specific-work output per stage are given in table III.

(8) Values of rotor total efficiency were assumed, based on stage work and leakage characteristics, at a level such that the resulting turbine total- to static-pressure ratio would match the value computed in step (4). These values are given in table IV.

(9) Stage velocity diagrams were constructed satisfying the assumed stage work and flow conditions, the requirement that the rotor entering and leaving angles be equal, and the requirement that there be no annular or circumferential divergence of the flow across the rotor.

The assumptions made in steps (2) to (8) affected the velocity diagrams obtained in step (9). Conversely, the resulting flow velocities affected the values assumed in steps (2) to (8). An iterative process was therefore required to bring the assumptions into agreement with the resulting velocity diagrams. Stage area ratios were then computed from the gas properties and the percentage weight flow assumptions made for each stage. From these ratios, the turbine weight flow was computed such that the resulting turbine with an 8-inch mean diameter and 0.60-inch blade height would have a total admitted flow area of 300° around the rotor annulus.

DECLASSIFIED

DECLASSIFIED

APPENDIX B

ESTABLISHMENT OF DESIGN STATIC EFFICIENCY FOR FOUR-STAGE REENTRY TURBINE

The estimate of overall turbine static efficiency η required in step (3) of the turbine design procedure (appendix A) was obtained by adjusting the performance of the three-stage reentry turbine (ref. 1) by the following amounts estimated to account for the design differences between the two turbines:

Three-stage reentry turbine static efficiency η (ref. 1), ...	0.62
Estimated loss in static efficiency of the three-stage turbine due to	
Excessive weight flow and spillage (ref. 1)	0.02
No labyrinth seals at rotor hub (ref. 1)	0.02
Subtotal	0.66
Estimated difference in static efficiency between subject four-stage and reference three-stage turbine:	
Staging four times instead of three at a value of speed-work parameter λ of 0.16 (ref. 1)	[a]+0.04
Increased overall loading characteristics in going from values of speed-work parameter λ of 0.16 (ref. 1) to 0.128 (four-stage turbine)	[a]-0.03
Higher reentry duct losses resulting from the diffusing-type reentry system (four-stage turbine)	-0.03
Total	0.64

[a]Obtained from ref. 8.

DECLASSIFIED

DECLASSIFIED

APPENDIX C

SYMBOLS

g	gravitational constant, 32.17 ft/sec^2
Δh	specific-work output, Btu/lb
J	mechanical equivalent of heat, 778.16 ft-lb/Btu
N	rotational speed, rpm
P_r	turbine inlet-total- to exit-static-pressure ratio, p'_0/p_{15}
p	absolute pressure, lb/sq ft (except where noted)
R	gas constant, ft-lb/(lb)($^\circ$R)
s	blade spacing (pitch), in.
T	total temperature, $^\circ$R
t	blade throat, in.
U	blade speed, ft/sec
V	absolute gas velocity, ft/sec
V_j	ideal jet velocity corresponding to total- to static-pressure ratio across turbine, $\sqrt{2gJ\,\Delta h_{id}}$
W	relative gas velocity, ft/sec
w	weight-flow rate, lb/sec
α	blade-setting angle measured from tangential direction, deg
γ	ratio of specific heats
δ	ratio of turbine-inlet pressure to NACA standard sea-level pressure, $p'_0/2116$
ϵ	function of γ used to correct weight flow and torque to inlet conditions at standard sea-level atmosphere, $\epsilon = \frac{0.740}{\gamma}\left(\frac{\gamma+1}{2}\right)^{\gamma/(\gamma-1)}$
η	static efficiency, based on total- to static-pressure ratio across turbine
η_r	rotor total efficiency, based on total- to total-pressure ratio across each stage of rotor

DECLASSIFIED

DECLASSIFIED

θ_{cr} squared ratio of turbine-inlet-flow critical velocity to that of NACA standard sea-level atmosphere, $(V_{cr,0}/1019)^2$

λ speed-work parameter, $U_m^2/gJ\,\Delta h$

ν blade- to jet-speed ratio, U_m/V_j

ρ gas density, lb/cu ft

τ torque, in.-lb

φ blade blockage, φ = channel area/(blade cross-sectional area + channel area)

Subscripts:

av average

cr conditions corresponding to Mach number of 1

id ideal

m mean

p pumped

s stage

st station

t throat

u tangential component

x axial component

Superscript:

' absolute total state

Stations (see fig. 1):

a rotor housing, shaft side of rotor

b rotor housing, turbine inlet and exhaust side of rotor

0 turbine inlet

1 first-stage stator outlet

2 first-stage rotor outlet

DECLASSIFIED

DECLASSIFIED
CONFIDENTIAL

3	first reentry duct
4	second-stage stator inlet
5	second-stage stator outlet
6	second-stage rotor outlet
7	second reentry duct
8	third-stage stator inlet
9	third-stage stator outlet
10	third-stage rotor outlet
11	third reentry duct
12	fourth-stage stator inlet
13	fourth-stage stator outlet
14	fourth-stage rotor outlet
15	turbine exit

DECLASSIFIED
CONFIDENTIAL

DECLASSIFIED

REFERENCES

1. Evans, David G.: Design and Experimental Investigation of a Three-Stage Multiple-Reentry Turbine. NASA MEMO 1-16-59E, 1959.

2. Wong, Robert Y., Darmstadt, David L., and Monroe, Daniel E.: Investigation of a 4.0-Inch-Mean-Diameter Four-Stage Reentry Turbine for Auxiliary Power Drives. NASA TM X-152, 1960.

3. Evans, David G., Guthrie, William D., and Wasserbauer, Charles A.: Design and Performance of a Six-Stage 8-Inch-Mean-Diameter Reentry Turbine. NASA TM X-487, 1962.

4. Wong, Robert Y.: Experimental Investigation of a 5.25-Inch-Mean-Diameter Two-Stage Reentry Turbine Suitable for High-Energy Auxiliary Drive Applications. NASA TM X-474, 1961.

5. Stewart, Warner L., Wong, Robert Y., and Evans, David G.: Design and Experimental Investigation of Transonic Turbine with Slight Negative Reaction Across Rotor Hub. NACA RM E53L29A, 1954.

6. Whitney, Warren J., Monroe, Daniel E., and Wong, Robert Y.: Investigation of Transonic Turbine Designed for Zero Diffusion of Suction-Surface Velocity. NACA RM E54F23, 1954.

7. Hilsenrath, Joseph, et al.: Tables of Thermal Properties of Gases. Cir. 564, NBS, Nov. 1, 1955.

8. Stewart, Warner L.: Analytical Investigation of Multistage-Turbine Efficiency Characteristics in Terms of Work and Speed Requirements. NACA RM E57K22b, 1958.

DECLASSIFIED

DECLASSIFIED

TABLE I. - ASSUMED LOSSES IN TOTAL PRESSURE

Station	Stage	Component	Total-pressure ratio across component
0 - 1	First	Stator	0.97
2 - 3	First	Diffuser	.88
3 - 4	First	Reentry duct	1.00
4 - 5	Second	Stator	.97
6 - 7	Second	Diffuser	.93
7 - 8	Second	Reentry duct	1.00
8 - 9	Third	Stator	.97
10 - 11	Third	Diffuser	.93
11 - 12	Third	Reentry duct	1.00
12 - 13	Fourth	Stator	.97
14 - 15	Fourth	Diffuser	.94

TABLE II. - ASSUMED FLOW-LEAKAGE LOSSES

(PERCENT OF INLET FLOW)

Stage	Circumferential leakage pumped between stages, percent		Labyrinth leakage, percent				Stator weight flow, percent
			Upstream side of rotor		Downstream side of rotor		
	In	Out	In	Out	In	Out	
1	3	20	-	2	-	2	100
2	20	12	-	1	-	1	79
3	12	6	1	-	1	-	85
4	6	3	2	-	2	-	93

DECLASSIFIED

DECLASSIFIED
CONFIDENTIAL

TABLE III. - ASSUMED EQUIVALENT SPECIFIC-WORK OUTPUT AND SPEED-WORK PARAMETER PER STAGE

Stage	Stage equivalent specific-work output, $\Delta h_s/\theta_{cr,0}$, Btu/lb	Speed-work parameter per stage, λ_s
1	16	0.37
2	14	.42
3	13	.46
4	13	.47
Total	56	

TABLE IV. - ASSUMED ROTOR TOTAL EFFICIENCY PER STAGE

Stage	Rotor total efficiency, η_r'
1	0.80
2	.82
3	.82
4	.80

DECLASSIFIED
CONFIDENTIAL

DECLASSIFIED
CONFIDENTIAL

TABLE V. - DESIGN-POINT PERFORMANCE RESULTS

Parameter	Performance at -		
	NACA equivalent air conditions	Cold-air test conditions	Example hot-operating condition with liquid-hydrogen and liquid-oxygen propellants
Inlet-total temperature, T'_0, °R	518.7	740	1860
Inlet-total pressure, p'_0, lb/sq in. abs	14.7	65	600
Gas constant, R, ft-lb/(lb)(°R)	53.38	53.38	379
Ratio of specific heats, γ	1.402	1.398	1.355
θ Performance-correction factors (see symbol list)	1	1.425	25.13
δ	1	4.423	40.83
ϵ	1	1.002	1.019
	Computed turbine performance[a]	Measured turbine performance	Computed turbine performance[a]
Specific work output, Δh, Btu/lb	44	63	1105
Weight flow, w, lb/sec	0.118	0.436	0.944
Rotational speed, N, rpm	11,040	13,180	55,300
Blade speed, U_m, ft/sec	385	460	1930
Total- to static-pressure ratio, P_r	20.5	20.5	16.95
Torque, τ, in.-lb	42.15	186	1690
Horsepower, hp	7.4	38.9	1484

[a]Computation based on cold-air test performance.

DECLASSIFIED
CONFIDENTIAL

DECLASSIFIED
CONFIDENTIAL

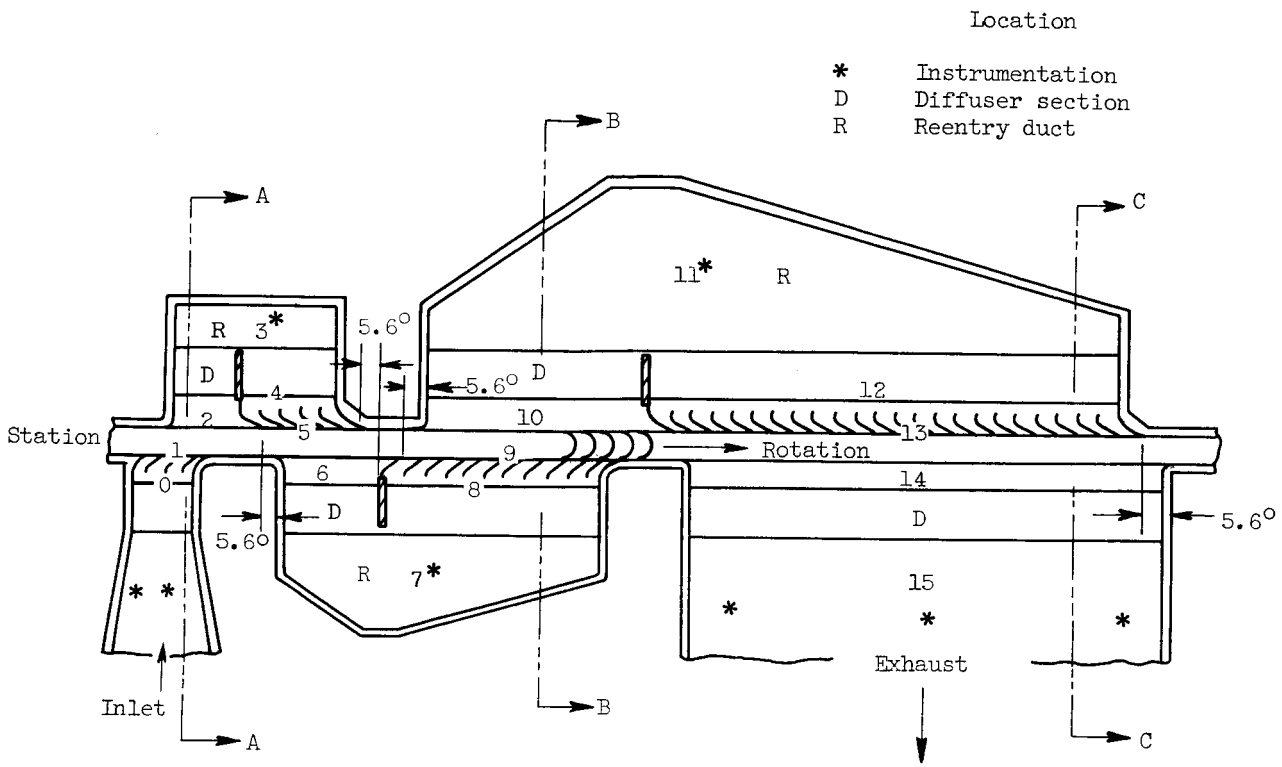

Turbine two-dimensional layout

Section A-A Section B-B Section C-C

Figure 1. - Schematic diagram of four-stage 8-inch-mean-diameter reverse-flow reentry turbine showing geometry, station number, and instrumentation location.

DECLASSIFIED
CONFIDENTIAL

DECLASSIFIED
CONFIDENTIAL

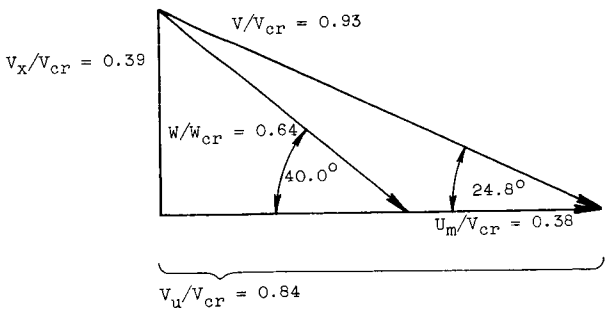

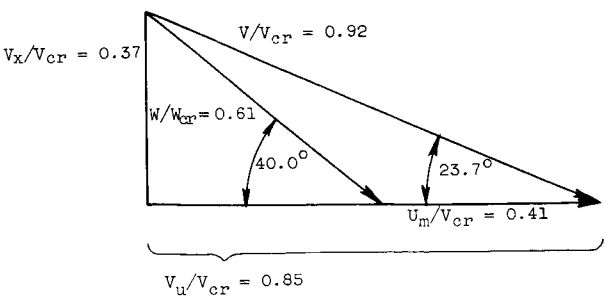

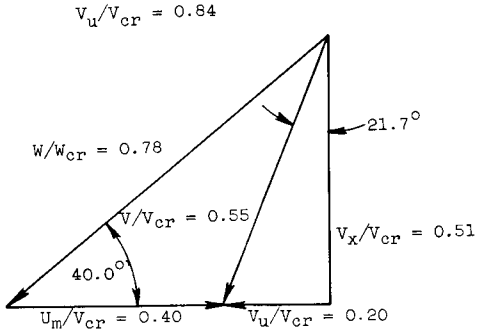

First stage, stations 1 and 2

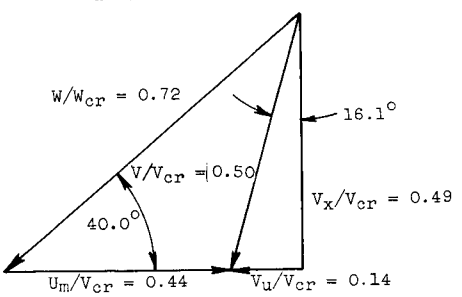

Second stage, stations 5 and 6

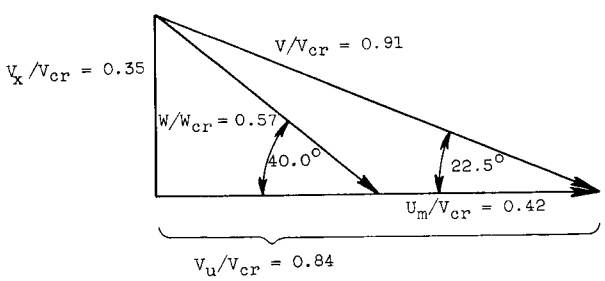

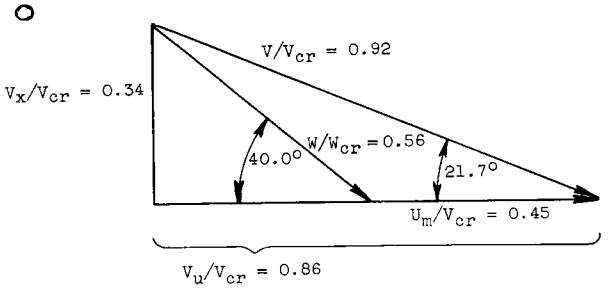

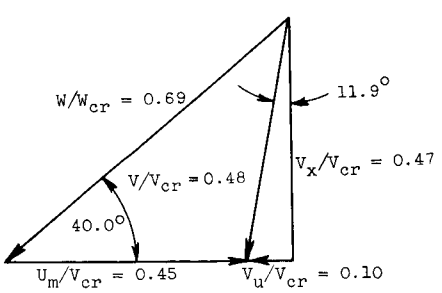

Third stage, stations 9 and 10

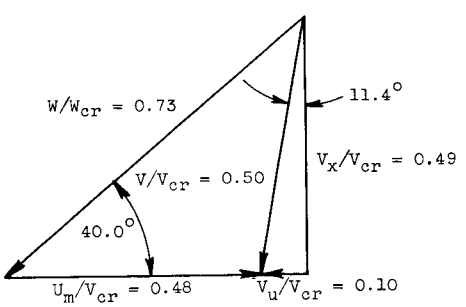

Fourth stage, stations 13 and 14

Figure 2. - Design free-stream velocity diagrams.

DECLASSIFIED
CONFIDENTIAL

DECLASSIFIED
CONFIDENTIAL

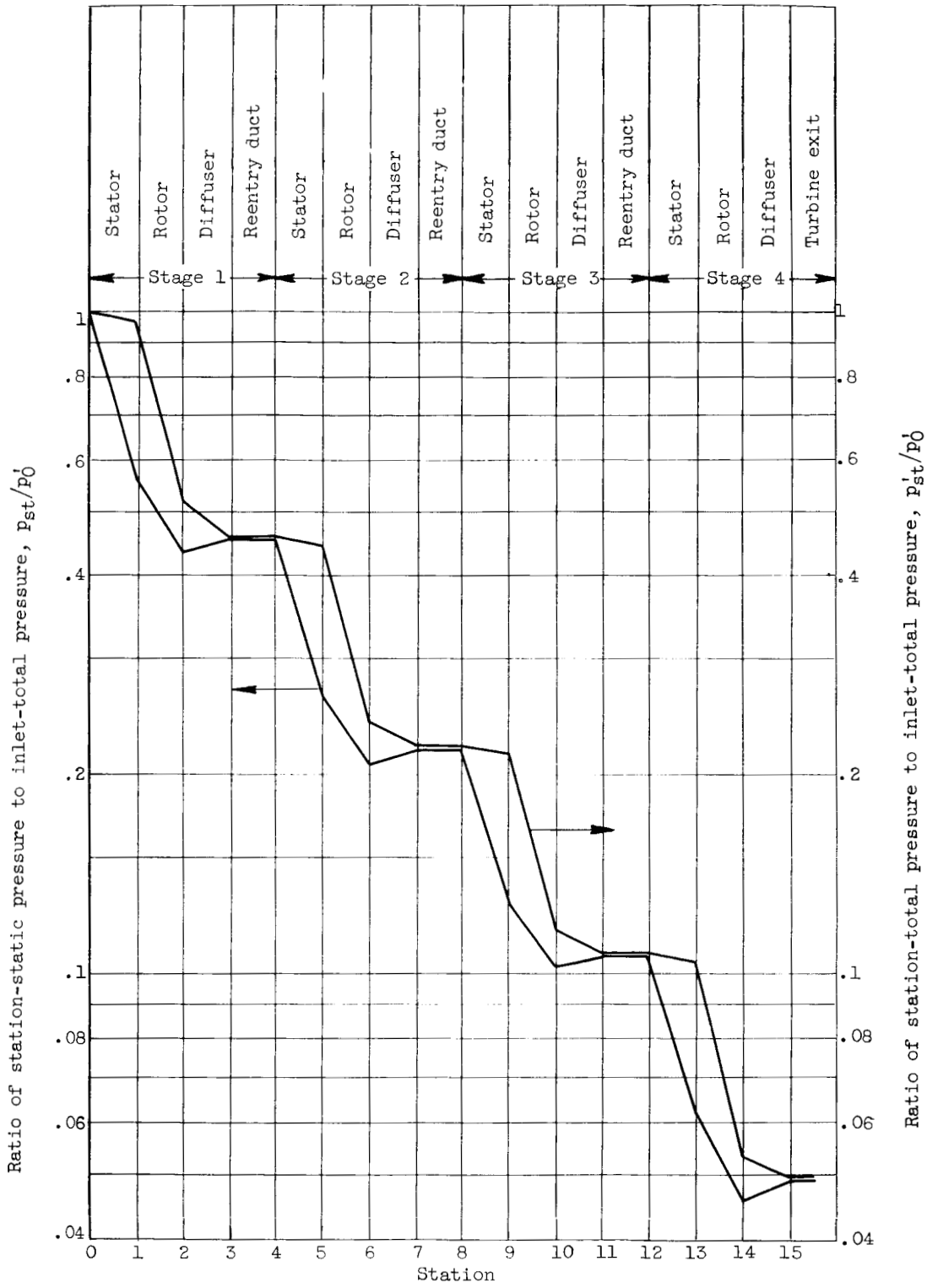

Figure 3. - Design variation of ratio of static and total pressure to inlet-total pressure across turbine. Pressure variations across rotor are absolute, not relative to rotor.

DECLASSIFIED
CONFIDENTIAL

DECLASSIFIED
CONFIDENTIAL

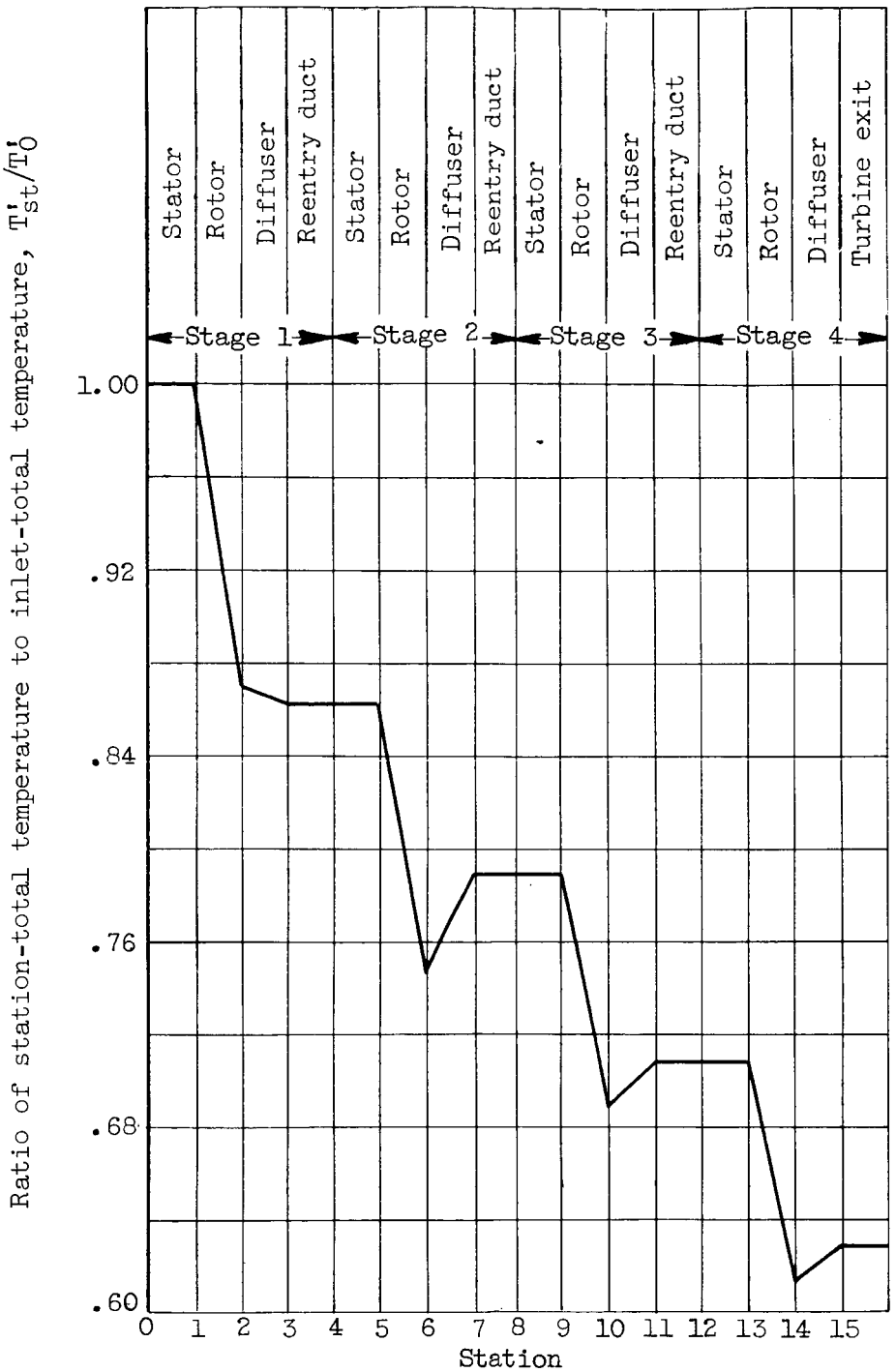

Figure 4. - Design variation of ratio of station-total to inlet-total temperature across turbine. Temperature variations across rotor are absolute, not relative to rotor.

DECLASSIFIED
CONFIDENTIAL

DECLASSIFIED
CONFIDENTIAL

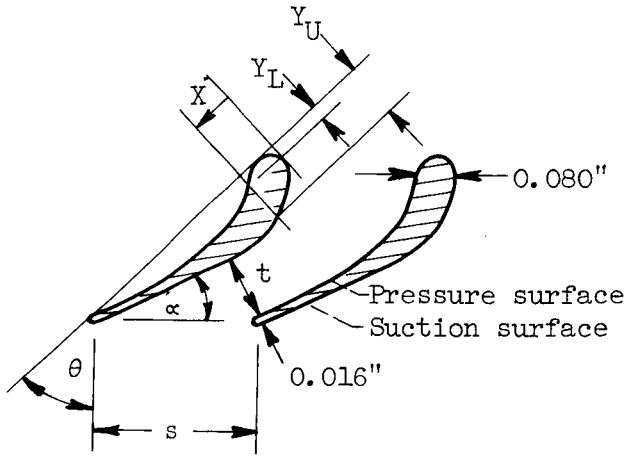

Stator section; stator blade heigth, 0.600 inch

X	Y_L	Y_U
0.0	0.040	0.040
.050	.001	.112
.100	.026	.129
.150	.044	.128
.200	.054	.115
.250	.056	.100
.300	.051	.085
.350	.042	.070
.400	.030	.054
.450	.018	.038
.500	.004	.023
.523	.008	.008

Stator blade coordinates for all stages: hub, mean, and tip (full size)

Specification	Stage				Total
	1	2	3	4	
α, deg	27.4	26.2	25.5	24.3	-------
s, in.	0.360	0.343	0.334	0.337	-------
t, in.	.149	.135	.127	.122	-------
Number of channels	4	7	16	35	-------
Total throat area, $in.^2$	.358	.567	1.220	2.562	-------
Total degrees of admission, deg	20° 35'	34° 22'	76° 30'	168° 36'	300° 3'
Admission, percent	5.72	9.55	21.24	46.82	83.33
θ, deg	45° 10'	46° 22'	47° 4'	48° 16'	-------

Stator spacing, angles, and throat areas

Figure 5. - Design mean-diameter stator spacing, angles, throat areas, and blade coordinates.

DECLASSIFIED
CONFIDENTIAL

DECLASSIFIED
CONFIDENTIAL

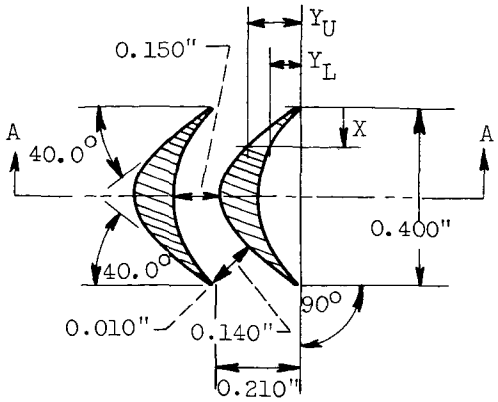

(a) Rotor mean-diameter section.

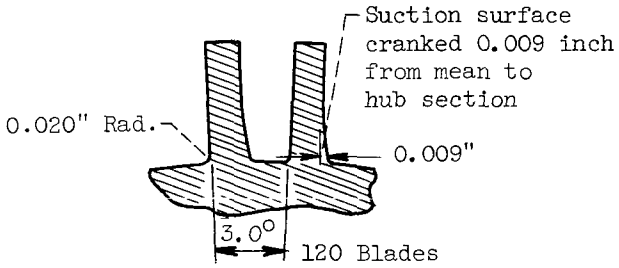

(b) Section A-A.

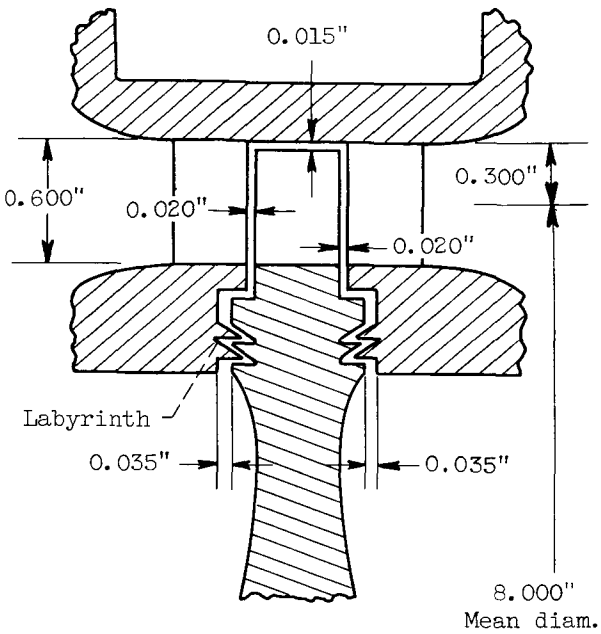

(c) Running clearances.

X	Rotor section diameter, in.			
	7.440		7.984 & 8.570	
	Y_L	Y_U	Y_L	Y_U
0.000	0.009	0.009	0.005	0.005
.020	.006	.036	.010	.030
.040	.020	.058	.023	.053
.060	.032	.078	.036	.072
.080	.042	.095	.047	.089
.100	.051	.109	.055	.103
.120	.058	.121	.063	.115
.140	.064	.129	.068	.123
.160	.068	.135	.071	.129
.180	.070	.138	.074	.132

X	Rotor section diameter, in.			
	7.440		7.984 & 8.570	
	Y_L	Y_U	Y_L	Y_U
0.200	0.071	0.139	0.074	0.133
.220	.070	.138	.074	.132
.240	.068	.135	.071	.129
.260	.064	.129	.068	.123
.280	.058	.121	.063	.115
.300	.051	.109	.055	.103
.320	.042	.095	.047	.089
.340	.032	.078	.036	.072
.360	.020	.058	.023	.053
.380	.006	.036	.010	.030
.400	.009	.009	.005	.005

(d) Rotor-blade coordinates.

Figure 6. - Design rotor geometry.

DECLASSIFIED
CONFIDENTIAL

DECLASSIFIED
CONFIDENTIAL

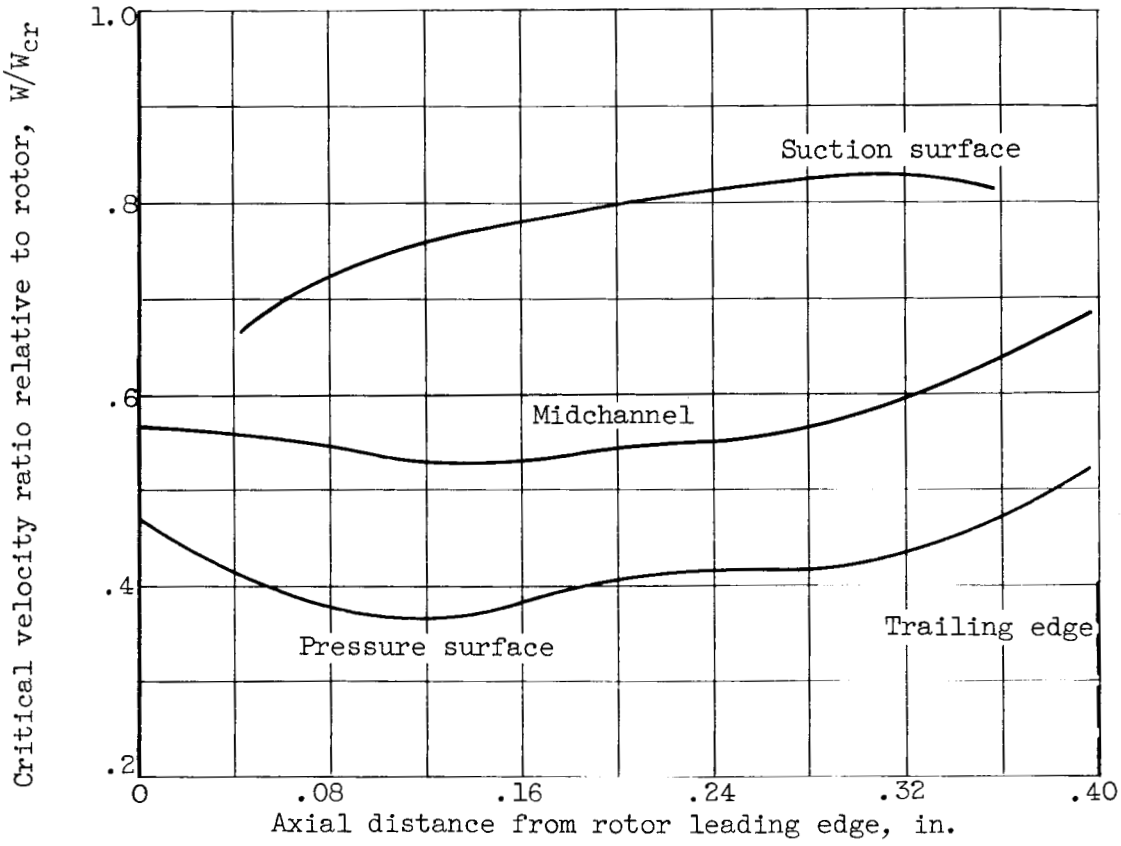

Figure 7. - Design mean-diameter rotor-channel velocity distribution for fourth stage.

DECLASSIFIED
CONFIDENTIAL

DECLASSIFIED
CONFIDENTIAL

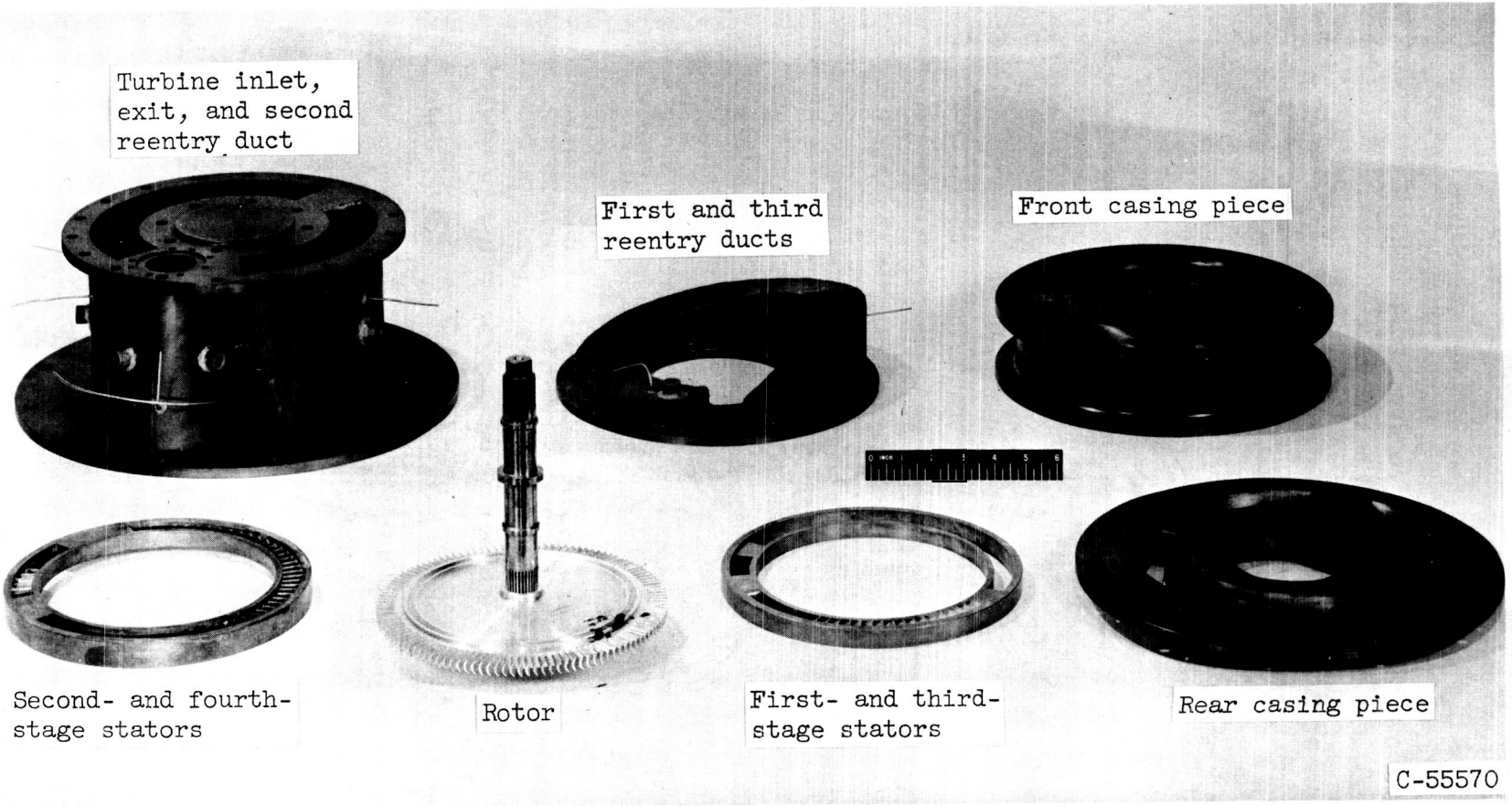

Figure 8. - Turbine components.

CONFIDENTIAL
DECLASSIFIED

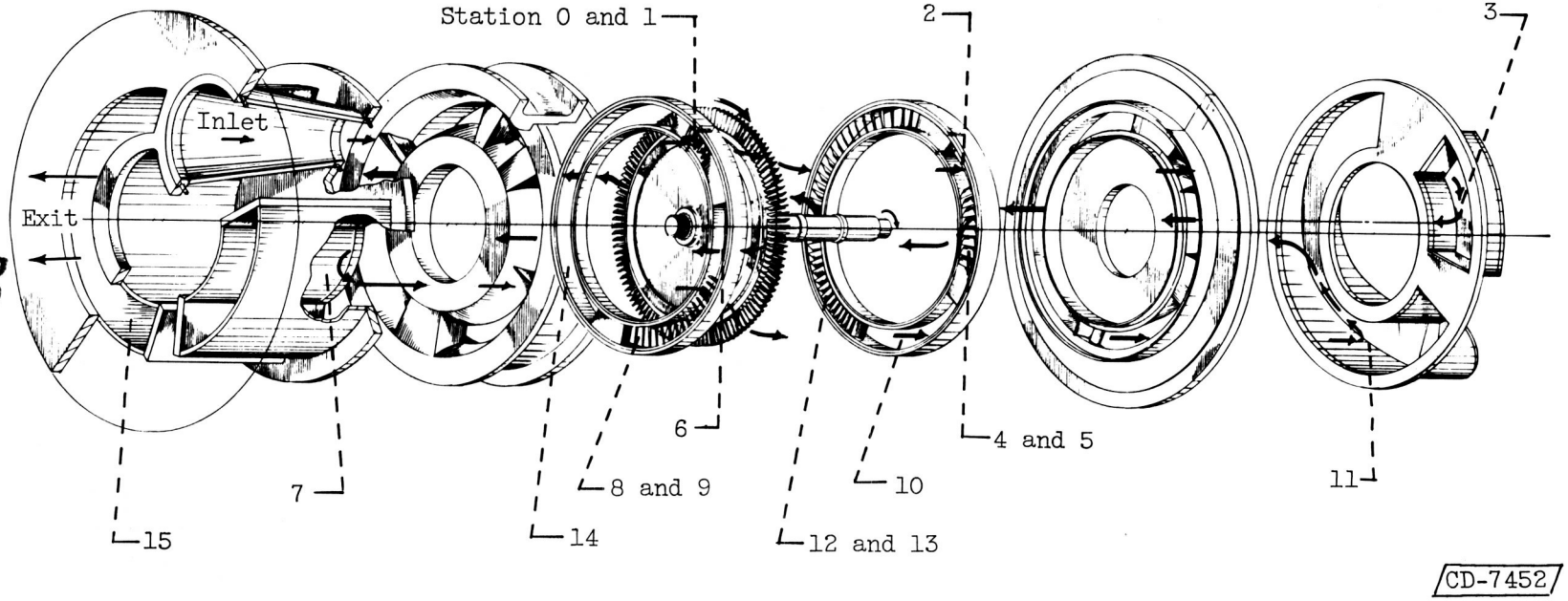

DECLASSIFIED
CONFIDENTIAL

Figure 9. - Exploded drawing of turbine components.

DECLASSIFIED
CONFIDENTIAL

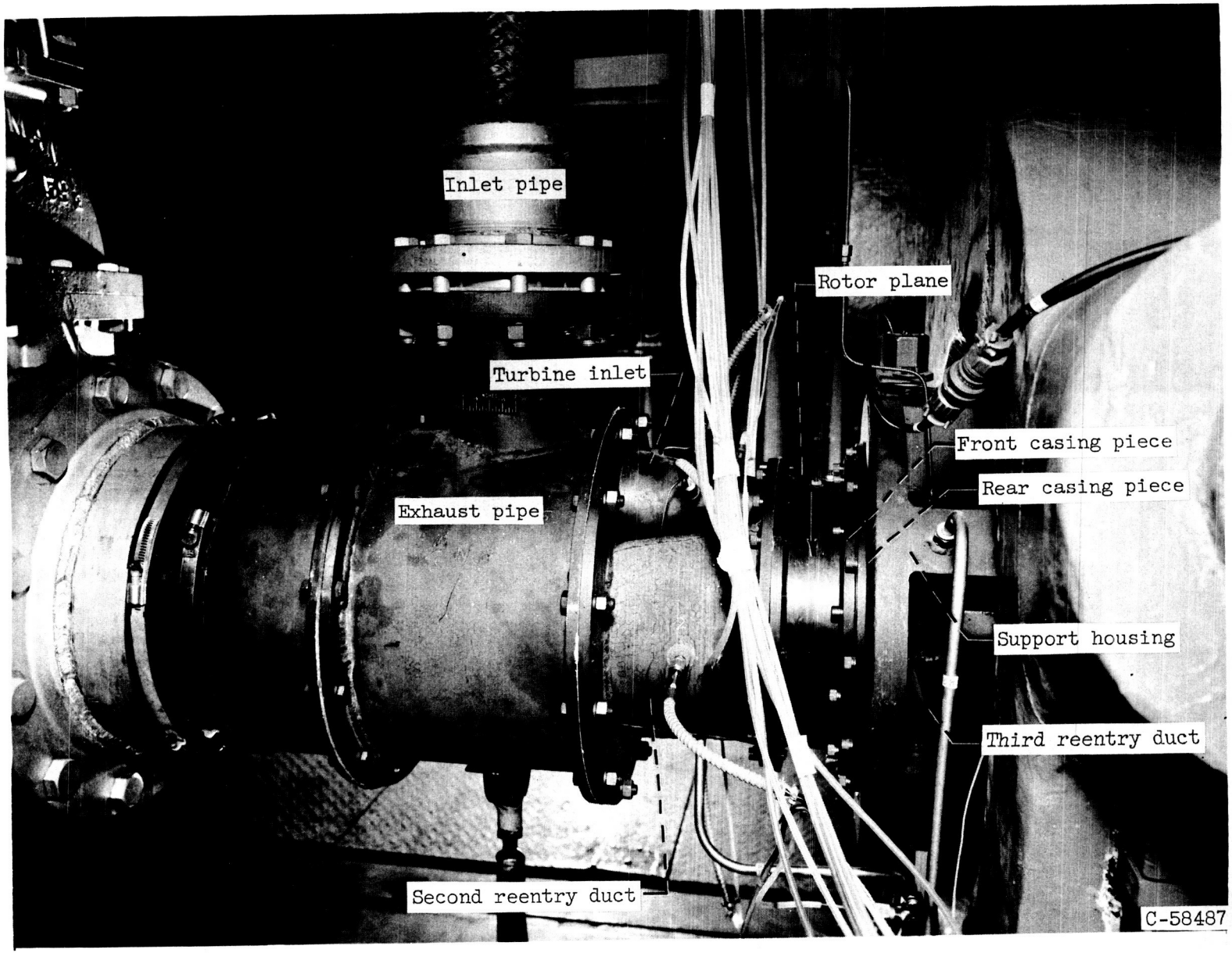

Figure 10. - Assembled turbine in test facility.

DECLASSIFIED
CONFIDENTIAL

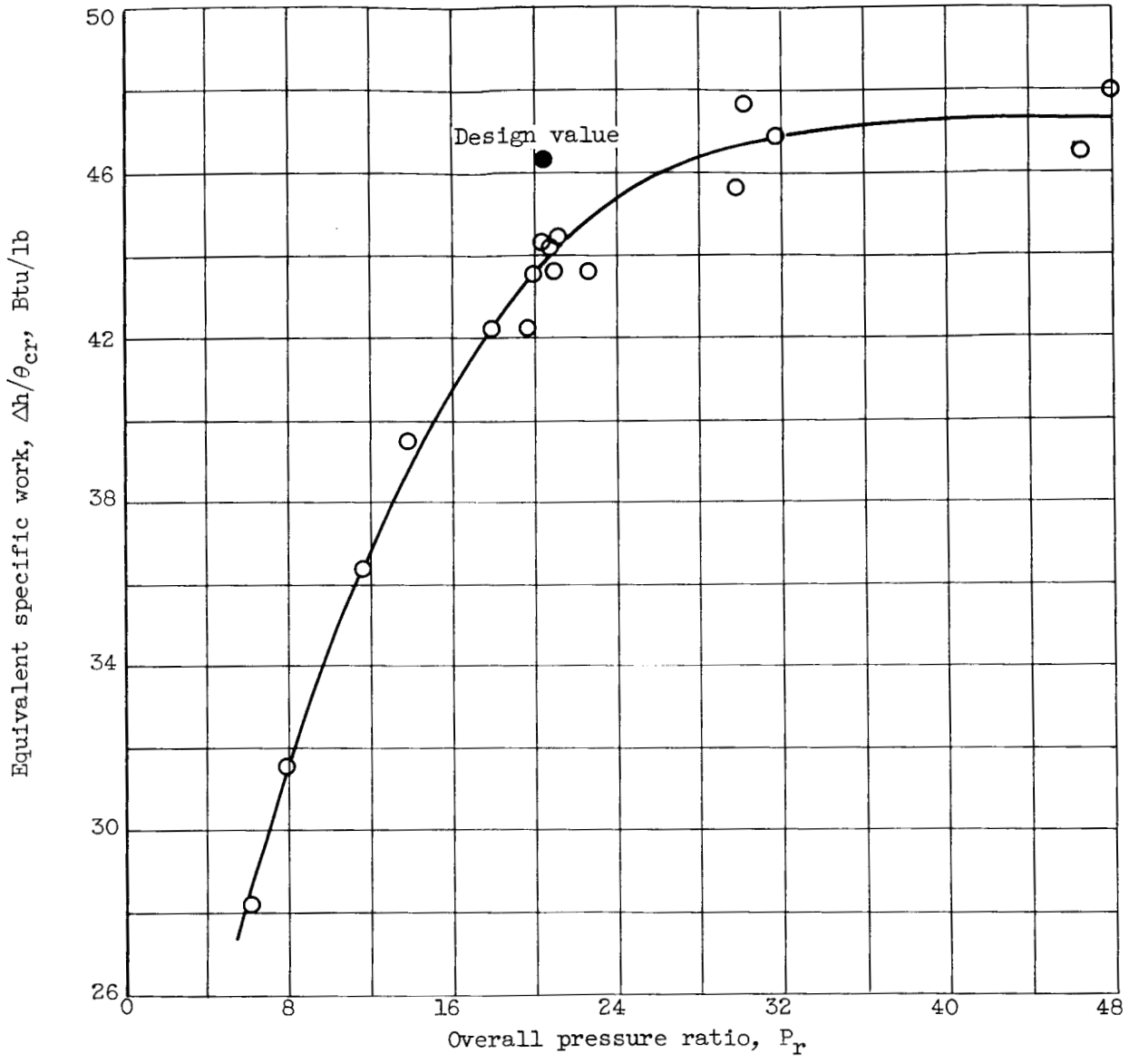

Figure 11. - Variation of equivalent specific-work output with overall pressure ratio at design speed.

DECLASSIFIED
CONFIDENTIAL

DECLASSIFIED
CONFIDENTIAL

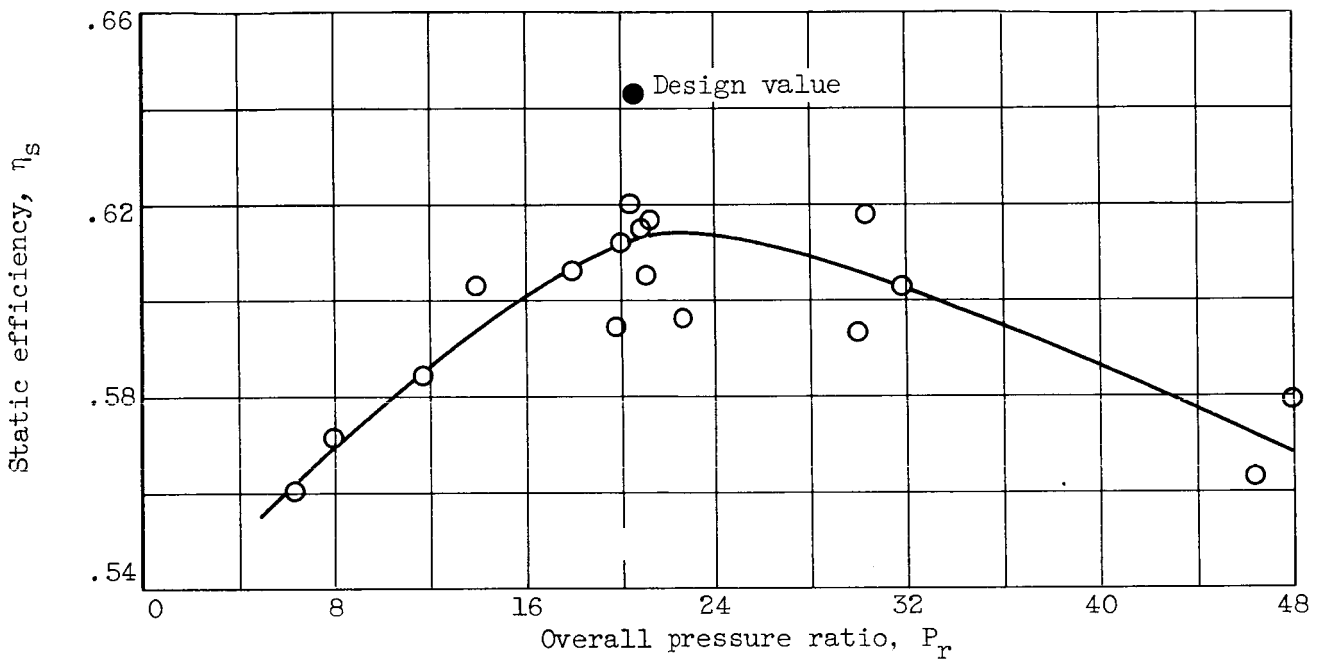

Figure 12. - Variation of static efficiency with overall pressure ratio at design speed.

DECLASSIFIED
CONFIDENTIAL

DECLASSIFIED
CONFIDENTIAL

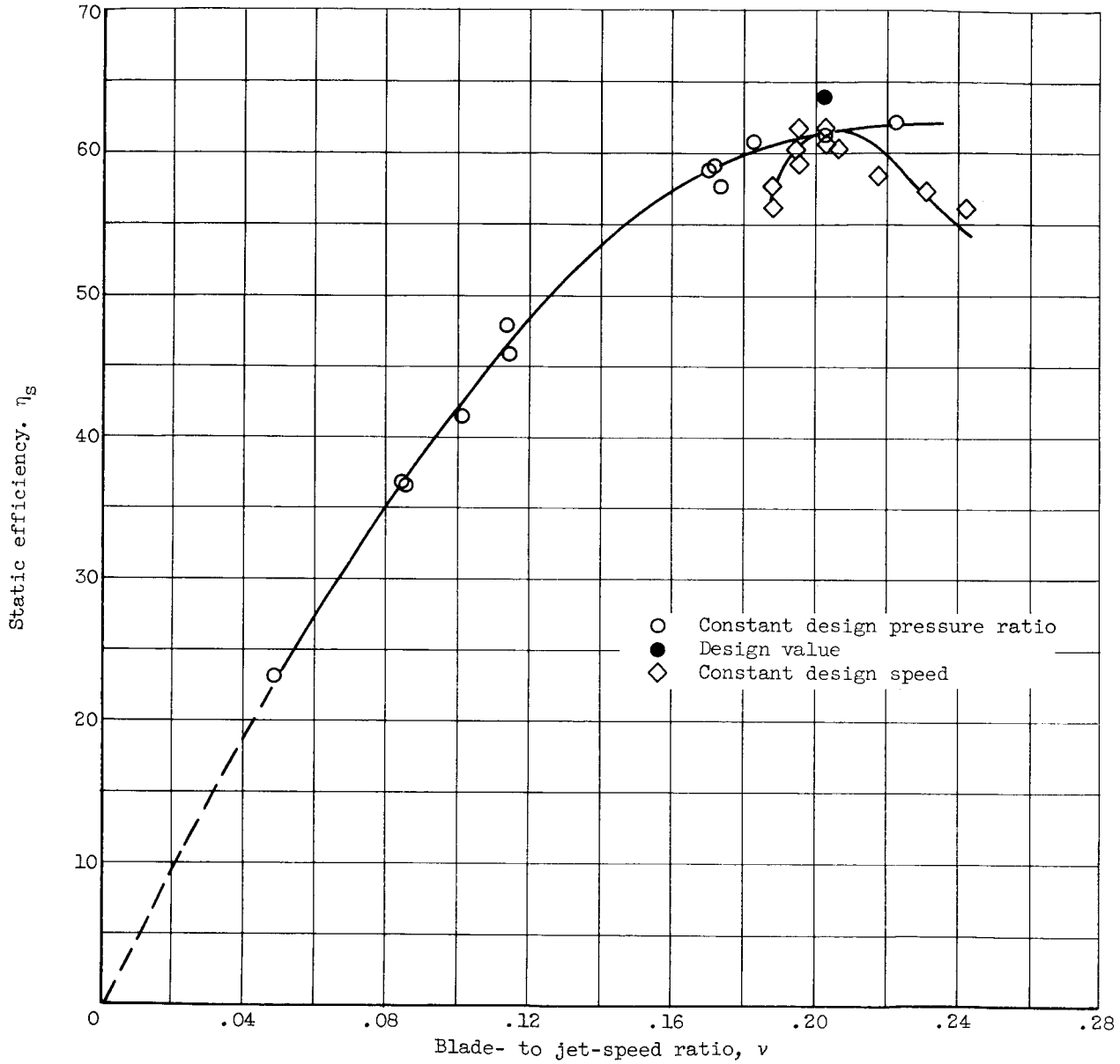

Figure 13. - Variation of static efficiency with blade- to jet-speed ratio.

DECLASSIFIED
CONFIDENTIAL

DECLASSIFIED
CONFIDENTIAL

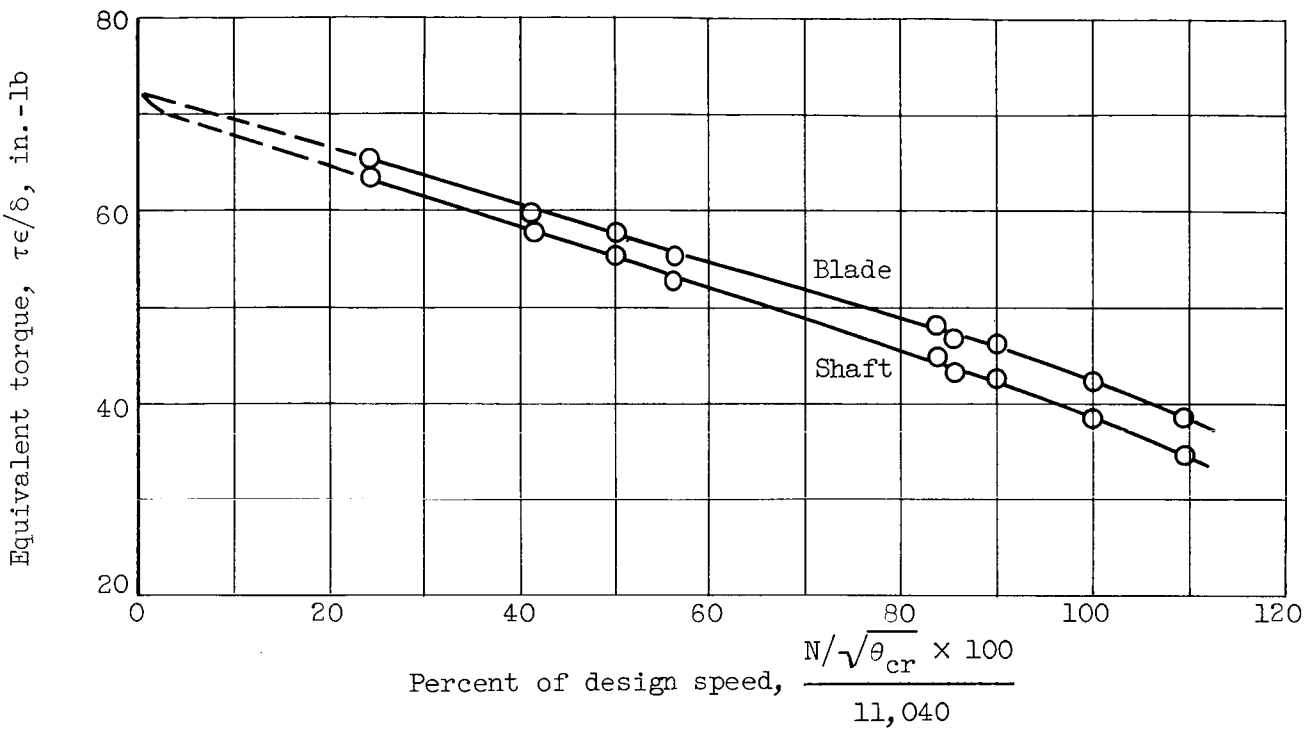

Figure 14. - Variation of equivalent torque with percent design speed at design pressure ratio.

DECLASSIFIED
CONFIDENTIAL

DECLASSIFIED
CONFIDENTIAL

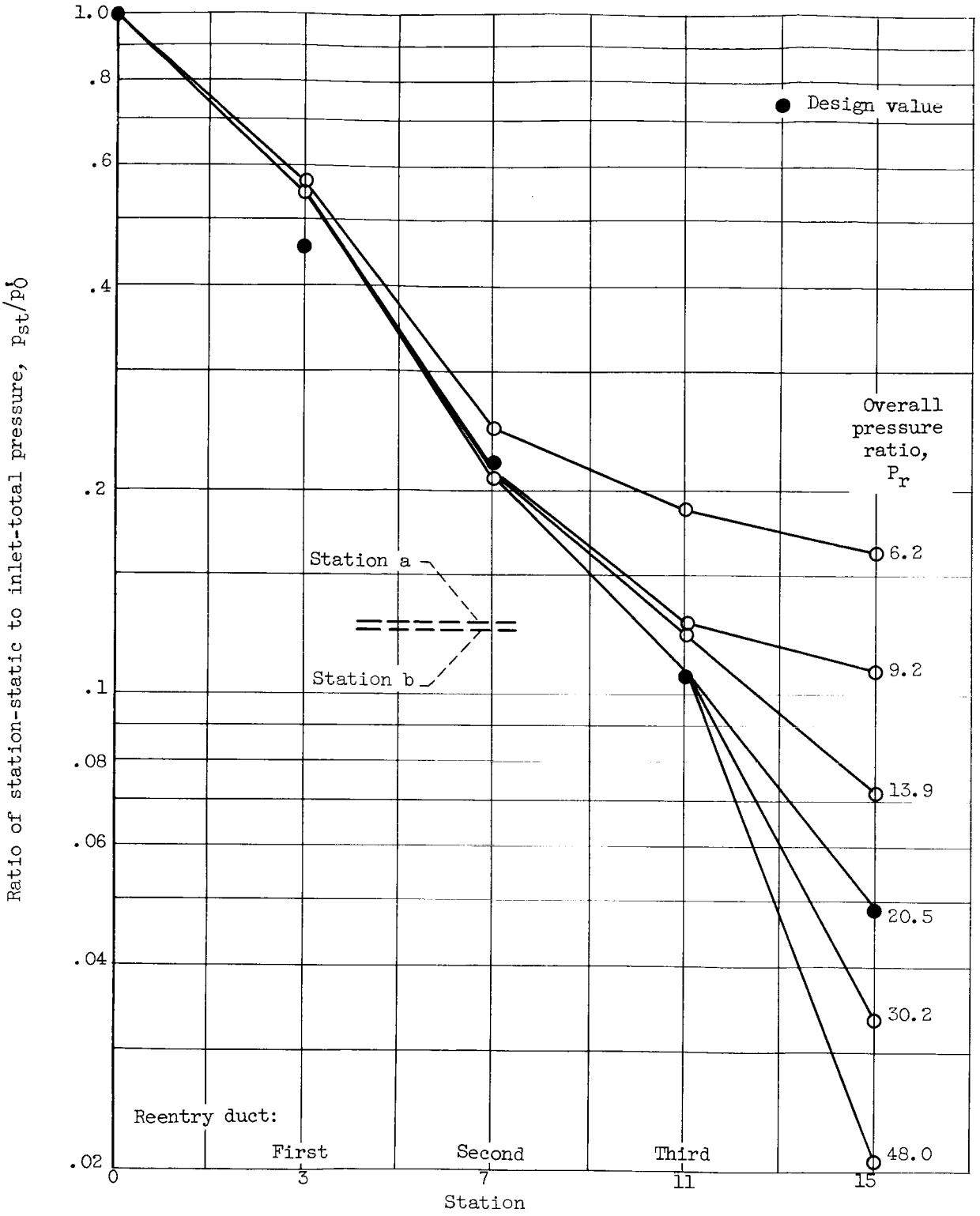

Figure 15. - Variation of station-static- to inlet-total-pressure ratio in each reentry duct with overall pressure ratio at design speed.

CONFIDENTIAL
DECLASSIFIED

DECLASSIFIED
CONFIDENTIAL

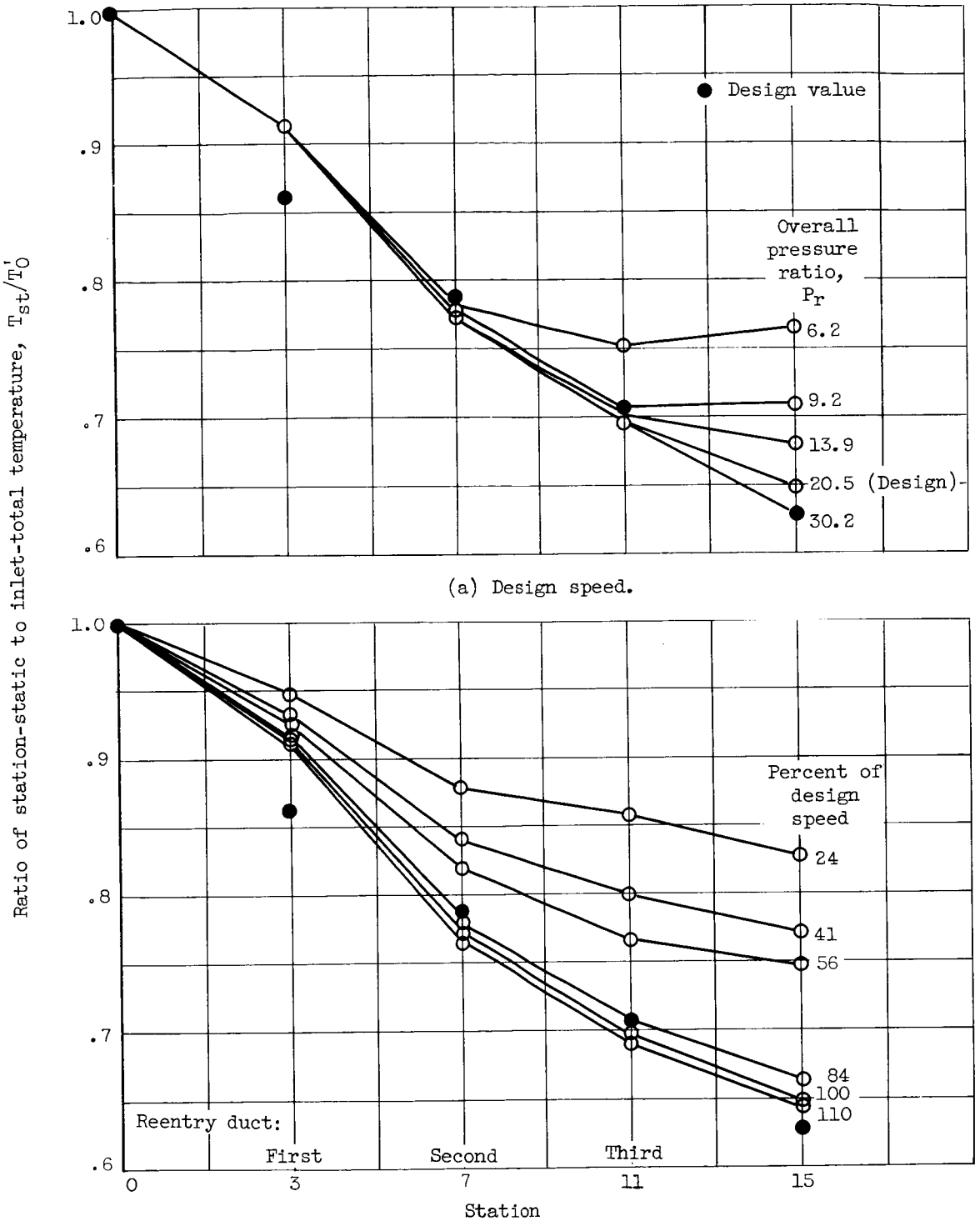

(a) Design speed.

(b) Design pressure ratio.

Figure 16. - Variation of station-static- to inlet-total-temperature ratio across turbine over the range of speeds and pressure ratios investigated.

DECLASSIFIED
CONFIDENTIAL